ISPRS Journal of Photogrammetry and Remote Sensing 79 (2013) 44–52

Contents lists available at SciVerse ScienceDirect

ISPRS Journal of Photogrammetry and Remote Sensing

journal homepage: www.elsevier.com/locate/isprsjprs

Spatiotemporal dynamic of surface water bodies using Landsat time-series data from 1999 to 2011

Mirela G. Tulbure [a,*], Mark Broich [b]

[a] Australian Wetlands, Rivers and Landscapes Centre, School of Biological, Earth and Environmental Sciences, University of New South Wales, Sydney, NSW 2052, Australia
[b] Plant Functional Biology and Climate Change Cluster, University of Technology Sydney, Broadway, NSW 2007, Australia

ARTICLE INFO

Article history:
Received 22 March 2012
Received in revised form 15 January 2013
Accepted 31 January 2013
Available online 16 March 2013

Keywords:
Optical remote sensing
Surface water body detection
Large area wetland inventory
Swan Coastal Plain
Western Australia
Long term trends

ABSTRACT

Detailed information on the spatiotemporal dynamic in surface water bodies is important for quantifying the effects of a drying climate, increased water abstraction and rapid urbanization on wetlands. The Swan Coastal Plain (SCP) with over 1500 wetlands is a global biodiversity hotspot located in the southwest of Western Australia, where more than 70% of the wetlands have been lost since European settlement. SCP is located in an area affected by recent climate change that also experiences rapid urban development and ground water abstraction. Landsat TM and ETM+ imagery from 1999 to 2011 has been used to automatically derive a spatially and temporally explicit time-series of surface water body extent on the SCP. A mapping method based on the Landsat data and a decision tree classification algorithm is described. Two generic classifiers were derived for the Landsat 5 and Landsat 7 data. Several landscape metrics were computed to summarize the intra and interannual patterns of surface water dynamic. Top of the atmosphere (TOA) reflectance of band 5 followed by TOA reflectance of bands 4 and 3 were the explanatory variables most important for mapping surface water bodies. Accuracy assessment yielded an overall classification accuracy of 96%, with 89% producer's accuracy and 93% user's accuracy of surface water bodies. The number, mean size, and total area of water bodies showed high seasonal variability with highest numbers in winter and lowest numbers in summer. The number of water bodies in winter increased until 2005 after which a decline can be noted. The lowest numbers occurred in 2010 which coincided with one of the years with the lowest rainfall in the area. Understanding the spatiotemporal dynamic of surface water bodies on the SCP constitutes the basis for understanding the effect of rainfall, water abstraction and urban development on water bodies in a spatially explicit way.

1. Introduction

Large scale wetland inventories and knowledge of wetland distribution and dynamic in space and time are essential for their management and conservation planning (Finlayson et al., 1999; Pressey and Adam, 1995; Zedler and Kercher, 2005). Wetlands provide a wide range of ecosystem services such as water supply and purification, carbon sequestration, flood and climate regulation, and coastal protection (Millenium Ecosystem Assessment, 2005; Mitsch and Gosselink, 1993). However, they are among the most threatened ecosystems in the world and changes in land use and land cover exacerbated by global climate change are contributing to their decline (Davis et al., 2010; Finlayson et al., 2011; Millennium Ecosystem Assessment, 2005). While under the Ramsar Convention wetlands encompass areas of marsh, fen, peatland or water, natural or artificial, permanent or temporary (UNESCO, 1971), here we focused on surface water bodies which comprise basin wetlands and estuaries (*sensu* Hill et al., 1996) as they represent the vast majority of wetlands in the study area, the Swan Coastal Plain (SCP). The SCP includes a biodiversity hotspot of global importance and is one region most vulnerable to climate change impacts given that rainfall has dropped by 15% since 1997 (Braganza and Church, 2011; Cleugh et al., 2011). Wetlands on the SCP retain significant biodiversity values (e.g., breeding habitat for waterbirds) and several of them are of national and international importance (e.g., Forrestdale and Thomsons Lakes). More than 70% of the wetlands on the SCP have been lost since European settlement in the early 1800s due to land clearing for urban development and agriculture and increased water abstraction (Davis and Froend, 1999). The major threats to wetlands on the SCP at present are declining surface water level caused by direct (e.g., reduced rainfall in the past decades, Braganza and Church, 2011) and indirect (e.g., increased evapotranspiration) effects of climate change, increase in groundwater abstraction for domestic, industrial and commercial consumption and changes in land use and

* Corresponding author.
E-mail address: Mirela.Tulbure@unsw.edu.au (M.G. Tulbure).

0924-2716/$ - see front matter © 2013 International Society for Photogrammetry and Remote Sensing, Inc. (ISPRS) Published by Elsevier B.V. All rights reserved.
http://dx.doi.org/10.1016/j.isprsjprs.2013.01.010

land cover due to rapid urban sprawl in the Perth metropolitan area (Froend and Sommer, 2010; Horwitz et al., 2008; Sommer and Horwitz, 2009; Weller, 2009). The number and size of surface water bodies are naturally dynamic in space and time (Alsdorf et al., 2007) and most wetlands on the SCP experience seasonal dynamic, with winter filling and summer drawdown (Townley et al., 1993). Baseline knowledge of the natural dynamics of surface water in space and time is needed to quantifying their decline.

Satellite remote sensing records synoptic data across space and time making it suitable for mapping and monitoring the extent and distribution of wetlands across large geographic areas and Landsat imagery has been commonly used for this purpose (Ozesmi and Bauer, 2002). Water extent can be mapped and quantified as the infrared and visible bands on the Thematic Mapper (TM) and Enhanced Thematic Mapper Plus (ETM+) on Landsat 5 and 7, respectively allow the separation of surface water from the land surface. Band 5 (wavelength 1.55–1.75 μm) is sensitive to water content in vegetation and soil as water absorbs most of the incoming radiation in this wavelength domain (Frazier and Page, 2000; Kingsford et al., 2004; USGS, 2003). The other two Landsat infrared bands, band 7 (wavelength 2.09–2.35 μm, (Smith, 1997) and band 4 (0.75–0.90 μm) have been used to map water bodies (Johnston and Barson, 1993).

Image data from both the TM and ETM+ sensors have been previously used for mapping wetlands in various areas such the Yellowstone National Park, USA, New South Wales, Australia and The Democratic Republic of Congo in Central Africa (Baker et al., 2006, 2007; Bwangoy et al., 2010; Kingsford et al., 2004; Wright and Gallant, 2007). Previous studies were based on two or a few time steps of cloud free images (e.g., flooding or drought) or image composites that were aggregated from multiple cloud affected images into a cloud free representation (Frohn et al., 2009; Kingsford et al., 2004; Wright and Gallant, 2007). With the opening of the USGS/EROS Landsat archive as of September 2010 (Williams et al., 2006), new monitoring and mapping opportunities for aquatic systems are provided. Previous studies were mostly based on a few time steps because of limited project budgets for purchasing data. Free access to the USGS/EROS archive now allows analysing the entirely systematically acquired record of Landsat imagery. Here we present a method that utilizes 605 images acquired by Landsat 5 and 7 over a time interval between 1999 and 2011 for mapping surface water bodies on the SCP as a test bed. This area has been chosen as a test site because it experienced a climatic drying trend and rapid urban expansion. Quantifying surface water dynamics in this area is essential for planning purposes and biodiversity conservation. The last wetland inventory on the SCP has been conducted in 1996 (Hill et al., 1996) and the history of wetland dynamic and loss on the SCP is poorly documented and has not been quantified in a spatially and temporally explicit way.

The overall aims of our research were to (1) develop a spatially and temporally explicit time-series of water bodies by automatically mapping the extent of water bodies on the SCP utilizing the Landsat archive from 1999 to 2011; (2) analyze the intra and inter-annual patterns of surface water dynamics using landscape metrics.

2. Methods

2.1. Study area

The Swan Coastal Plain (SCP), an area of 36,000 km^2, is located in the southwest of Western Australia between the Darling Scarp to the east, and the Indian Ocean to the west (Fig. 1). It encompasses the Perth Coastal Plain and Dandaragan Plateau bioregions characterized by sandy soils of aeolian and alluvial origin

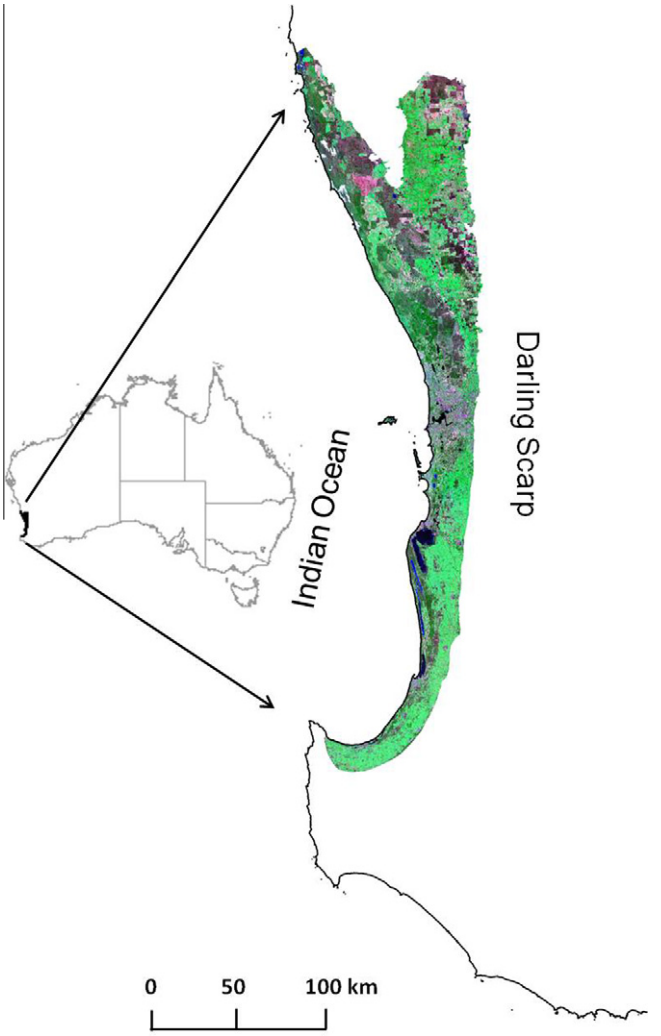

Fig. 1. Location of the Swan Coastal Plain study area in the southwest of Western Australia and a mosaic of Landsat 7 ETM+ images displayed as Red band 7 (2090–2350 nm), Green band 4 (770–900 nm), Blue band 2 (520–600 nm). (For interpretation of the references to colour in this figure legend, the reader is referred to the web version of this article.)

(Department of Sustainability, 2009). The SCP has a warm Mediterranean climate with hot dry summers and cool wet winters. Rainfall ranges between 600 and 1000 mm annually and most of it occurs in winter (May until October) when temperature is the lowest. Monthly average temperatures vary between 10 °C in mid winter to 25 °C in mid summer. The SCP is divided into three dune systems that run north-south parallel to the coastline and correspond to different geological units. The majority of water bodies on the SCP are shallow (<3 m deep), small (<100 m along the longest axis) permanent lakes or seasonal basin wetlands, commonly occurring in the inter-dunal depressions (Davis et al., 2010; Townley et al., 1993). Hill et al. (1996) recorded 10,000 basin and palusplain wetlands at the beginning of 1990s.

2.2. Data used and data processing

Fig. 2 overviews the methodological steps undertaken to produce a time-series of surface water bodies. We used imagery acquired by the Landsat Thematic Mapper (Landsat 5) and the Enhanced Thematic Mapper Plus (ETM+) (Landsat 7) sensors between 1999 and 2011. The sensors have an overpass frequency of 16 days. The SCP is covered by 6 Landsat World Reference System

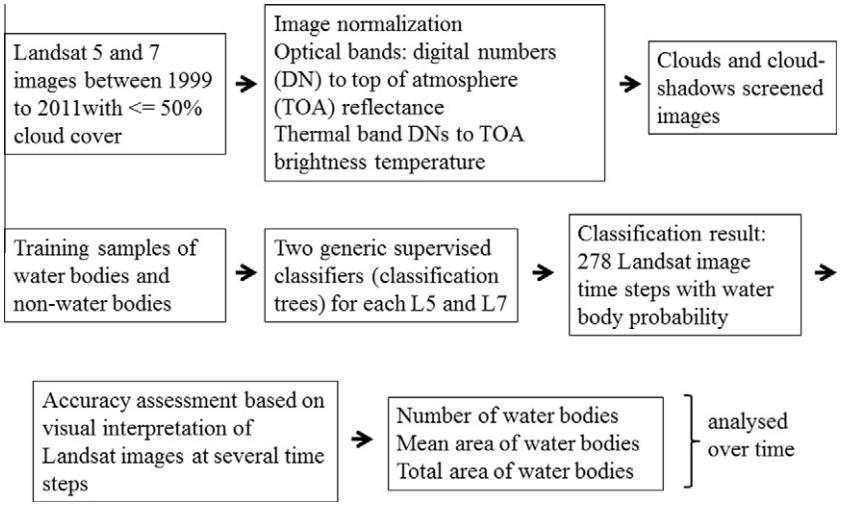

Fig. 2. Methodological overview showing the input data and the steps taken to produce a time-series of surface water bodies on the SCP, Western Australia.

path/row combinations (paths 112–113 and rows 81–83). We downloaded Level 1 terrain corrected (L1T) Landsat 5 and Landsat 7 images for the study period from USGS/EROS (http://landsat.usgs.gov/). The USGS/EROS L1T standard product is radiometrically and geometrically corrected and includes geometric correction for relief displacement (Roy et al., 2010). For the period from April 1999 to May 2003 we downloaded 159 Landsat 7 images. To represent the period after the Landsat 7 scan line corrector failure (June 2003–December 2011), we downloaded 446 Landsat 5 images. The Landsat 7 scan line corrector failure led to track-parallel data gaps that rendered 22% of each image unusable (Maxwell et al., 2007) and thus unsuitable for characterizing spatial-temporal dynamics of water bodies. In total, there were 278 image time steps for the study area derived from Landsat 5 and 7 imagery combined. We only downloaded images that had $\leqslant$50% cloud cover over the study area. Using this rule we sourced and processed 52% of all images available in the USGS/EROS archive. According to the metadata the average percent cloud cover of the selected images was 4% with 50% of the images cloud free.

We used ENVI/IDL 4.8 software (Exelis Visual Information Solutions, 2011) and R systems (R Development Core Team, 2008) to develop a generic classification model to automatically map surface water bodies. While it is possible to classify surface water bodies using a supervised or unsupervised classification for every image, deriving a generic supervised classifier applicable across space and time is less time consuming given the large number of images (605 images; an average of eight images per path-row and year). To enable mapping of water bodies with a generic classification model, imagery acquired over different location and at different points in time needed to be radiometrically normalized. We normalized the imagery by converting the optical bands' digital numbers (DN) to top of atmosphere (TOA) reflectance and the thermal band DNs to TOA brightness temperature using the equations and coefficients provided in Chander et al. (2009). Normalization aimed to correct for changes in the instrument radiometric calibration, and variations of sun–earth distance, exoatmospheric solar irradiance, and solar geometry between images acquired over different locations and at different times. We resampled the 120 m and 60 m thermal bands of TM and ETM+ respectively to the 30 m optical bands.

We used a classification tree algorithm trained across the study area and on images acquired at various points in time to account for seasonality. We selected training samples via photo interpretation of Landsat images. We selected training samples to represent both the spectral signature of water bodies and non-water areas across the study area and seasons. The training data sets included 75,000 pixels for the Landsat 5 model and 20,000 pixels for the Landsat 7 classification. This combination of radiometric image normalization and training across space and time allowed the derivation of a generic algorithm.

The training data were used to derive generic statistical classification rules with a supervised classification tree (CT) algorithm. CT approaches have been extensively used to characterize remotely sensed data sets across space and time (Baker et al., 2006, 2007; Broich et al., 2011a, 2011b; Brown de Colstoun et al., 2003; Friedl and Brodley, 1997; Hansen et al., 2008; Roy et al., 2010). The CT algorithm is a nonparametric classifier (it does not assume any distribution of the data) that predicts class membership for multiple explanatory variables. This is done by recursively splitting the training data into more homogeneous subsets ("nodes"). This recursive splitting selects a split point on an explanatory variable that separates the data into the most homogeneous subsets of the response variables (Breiman, 1996). The derived splitting rules are then applied to the entire dataset to be classified. The CT algorithm accommodates abrupt, non-monotonic and non-linear relationships between the explanatory and response variables (Breiman, 1996; Breiman et al., 1984). Explanatory variables consisted of TOA reflectance in every spectral band, brightness temperature, normalized difference vegetation index (NDVI), and the mean values within a 3×3 moving window for all of the above variables (Table 1). Two generic CT models were derived, one for each Landsat 5 and Landsat 7 data. Each model was applied to all pixels acquired by the respective sensor over the study period. The classification result was per pixel likelihoods of surface water for every image acquired over 13 years that were turned into time-series of surface water maps by thresholding per pixel likelihoods at 50%.

Optically thick clouds preclude Landsat surface observations (Roy et al., 2010). Areas affected by clouds, haze and cloud shadows were manually masked. While automated cloud and cloud shadow masking has been demonstrated for Landsat images (Broich et al., 2011a, 2011b; Hansen et al., 2008; Roy et al., 2010), water bodies are challenging to automatically differentiate from cloud shadows as spectra of shadows are highly variable and indistinguishable from those of water bodies. Thus, we opted for a manual masking approach which did not aim at per pixel flagging of clouds or shadows but masked wider areas affected by clouds and shadows.

Table 1
Explanatory variables used in the decision tree models based on Landsat 5 and 7.

Number	Variables	Number	Variables
1	TOA of band 1	9	Mean in a 3 × 3 window of TOA of band 1
2	TOA of band 2	10	Mean in a 3 × 3 window of TOA of band 2
3	TOA of band 3	11	Mean in a 3 × 3 window of TOA of band 3
4	TOA of band 4	12	Mean in a 3 × 3 window of TOA of band 4
5	TOA of band 5	13	Mean in a 3 × 3 window of TOA of band 5
6	TOA of band 7	14	Mean in a 3 × 3 window of TOA of band 7
7	Brightness temperature	15	Mean in a 3 × 3 window of Brightness temperature
8	NDVI	16	Mean in a 3 × 3 window of NDVI

We filled data gaps due to clouds and cloud shadows in a given image by inserting the most common classification result per pixel (surface water or non-water) for the respective season. This most common result was determined from the number of times a given pixel was observed as surface water in each season (winter, spring, summer and autumn beginning 1st of June, 1st of September, 1st of December, and 1st of March, respectively) over a period of three years (e.g. winter 1999–2001). For example, if clouds covered part of an image acquired in the winter of 2003, the cloud-obscured pixel was filled by the most common classification result for this pixel in winter for the 2002–2004 time period.

2.3. Accuracy assessment

To assess the accuracy of the surface water body time-series we randomly sampled three time steps for each of the four seasons (summer, autumn, winter, and spring) which resulted in twelve time steps that were used in the accuracy assessment. While ideally each time step would be sampled, it was logistically impractical to sample 278 time steps of the time-series. The temporal stratification by season was chosen to derive evaluation data across seasons and years. We used a stratified sampling design targeting areas where water bodies are expected to occur. The stratification was based on the geomorphic wetlands dataset mapped by the Department of Environment and Conservation (DEC) of Western Australia (Semeniuk and Semeniuk, 1995). For each of the 12 time steps we evaluated 100 pixels, with 50 pixels randomly selected within the area mapped as surface water bodies by DEC and 50 pixels randomly selected in the remaining area. This resulted in 1200 pixels being assessed.

By sampling within the area mapped as surface water bodies by DEC, we aimed to increase the chance of sampling the "rare" surface water body class, which according to our results only encompassed a maximum of 2.3% of the study area in winter of some years. This approach of specifically targeting the rare class is critical to the success of mapping projects when the rare class is of interest (Stehman and Czaplewski, 1998; Stehman et al., 2003). However, most errors in image classification are spatially concentrated at the boundaries between land cover classes rather than in the homogeneous class interior and are caused by the occurrence of mixed pixels along the class boundaries (Foody, 2002; Smith et al., 2003). Mixed pixels are caused by the boundary of land cover classes falling within pixels. To investigate the accuracy of the surface water body time-series, we buffered the edge of the mapped surface water bodies by 90 m on either side. Within the resulting 'edge' stratum that included both water and non-water, we randomly sampled 50 pixels for each of the 12 time steps. The aim of evaluating these additional 600 pixels was to specifically evaluate the areas where misclassification is most likely to occur. For each randomly sampled pixel, we derived reference data by visually interpreting the Landsat image for the sampled time step and labelled the pixel as water body or non-water body accordingly. We computed classification accuracies of the surface water body time-series as overall accuracy, user's and producer's accuracy of surface water bodies and non-surface water bodies using a confusion matrix (Foody, 2002).

2.4. Spatial configuration of water bodies

To quantify the spatial configuration of water bodies on the SCP across time we generated landscape metrics using FRAGSTATS (McGarigal et al., 2002). For the purpose of our study, four metrics (McGarigal et al., 2002) were generated using the surface water time-series. These metrics are commonly used in landscape ecology and depict the changes and dynamics of seasonally continuous surface water body time-series. Number of water bodies (NW) is a count of water bodies across the area. Mean surface water body area (MWA) is the summed area of all water bodies divided by the total number of water bodies: $MWA = \sum Xi/NW$, where X_i is the corresponding surface water body i within the landscape and NW is number of water bodies in the landscape. The coefficient of variation (CV) of MWA stands for the standard deviation of the MWA divided by the mean, multiplied by 100 to convert the rate to a percentage. Total area of water bodies (TAW) refers to the total area (m^2) of water bodies in the landscape.

3. Results

3.1. Classification tree results

Two classification tree models were applied for each Landsat 5 and Landsat 7 using sixteen explanatory variables (Table 1). The first most important variable in the Landsat 5 model was TOA reflectance of band 5, which explained 51% deviance followed by TOA reflectance of bands 4 and 3 which accounted for 20% and 12% of deviance reduction, respectively.

The first most important variable in the Landsat 7 model was TOA reflectance of band 5, which explained 56% deviance followed by TOA reflectance of bands 4 and 3 which accounted for 27% and 10% of deviance reduction, respectively. It is known that the infrared bands and the red band due to its relevance for vegetation quantification are most relevant for the classification of the land surface (Hansen and Loveland, 2012) including mapping of water bodies (Wright and Gallant, 2007). The reason for this is the increasing absorption of longer wavelengths by water. Short wavelength bands tend to have limited use due to the high level of atmospheric scattering.

3.2. Accuracy assessment of the time-series

For the combined sample of pixels inside and outside of the area mapped as surface water bodies by DEC (n = 1200) the overall classification accuracy was 97% and user's and producer's accuracies of surface water bodies were 98% and 93%, respectively (Table not shown). We visually identified 18.3% of the 1200 pixel sampled as surface water bodies showing that our stratification based on the DEC survey effectively targeted surface water. Inside and outside of the area mapped as surface water by DEC we flagged 35.5% and 1.2% of the sampled pixels as water, respectively. This showed that surface water bodies occurred outside of the area mapped as water bodies by DEC. The reverse was also true, the area mapped as surface water by DEC was not covered by water in every

time step sampled here. This is not surprising given that the DEC survey was conducted from aerial photography in the beginning of 1990s and seasonal and interannual fluctuations of surface water extent have occurred since then.

Within the 'edge' stratum, 34.3% of the 600 sample pixels were flagged as water. The resulting overall accuracy near the edge of land cover classes was 90% with a user's and producer's accuracy of the majority class (non surface water) being 91% and 94%, respectively (Table 2). The user's and producer's accuracy of surface water bodies was 89% and 84% respectively. We expected lower user's and producer's accuracies of surface water bodies when concentrating sampling effort along the edge of classes as this approach evaluates the accuracy specifically in areas were errors are most likely to occur rather than the entire study area. When combining the 1800 samples taken across the three strata (within the area mapped as surface water by DEC, outside of this area, and within 90 m of the mapped class boundary) the overall accuracy was 96% with a user's and producer's accuracy of non-water bodies of 96% and 98% respectively (Table 3). The user's and producer's accuracy of surface water bodies was 93% and 89%, respectively (Table 3).

3.3. Intra and interannual dynamic of surface water bodies

The number of water bodies on the SCP varied from a minimum of 871 in January 2009 to a maximum of 5069 in July 2005 (Fig. 3a). The number of water bodies showed high seasonal variability with highest numbers in winter when there was more surface water in the landscape and lower numbers in summer when the landscape on the SCP was dry (Figs. 3a and 4). The mean size of water bodies varied from 6.5 ha to 26.6 ha in June 2005 and January 2009, respectively (Fig. 3b). The mean size of water bodies showed seasonal variability with mean size of water bodies being highest in the southern hemisphere summer (February) and lowest in winter (August). The coefficient of variation of mean size also showed seasonal variability and was highest in winter and lowest in summer, which suggests that in summer most water bodies are larger in size, whereas in winter the size is more heterogeneous (Fig. 3b and c). There was a high positive correlation ($R^2 = 0.89$) between number of water bodies and variability in the water body size (Fig. 3a and c). The total water area in the SCP landscape varied from 22,404 ha in February 2003 to 35,671 ha in September 1999 (Fig. 3d) which represented 1.5% and 2.3% of the entire SCP, respectively. Total water area in the landscape showed high seasonal variability with highest values in winter and lowest in summer. While the seasonality in number of water bodies was high, the number and size of water bodies also showed variability in winter and summer across years (Fig. 5). Among years, an increase in number of water bodies can be observed in winter until 2005 after which a decline can be visually noted (Fig. 3a). The mean area of water bodies increased in winter after 2005, whereas the CV of mean water body area increased in winter until 2005 and decreased after 2005 and decreased in summer until 2005 and increased after that. The total water area decreased until February 2005 in both winter and summer, after which a sharper decline can be visually noted (Fig. 3d). In summary, all four landscape metrics showed intra and interannual dynamics of surface water bodies.

Table 2
The error matrix, overall, producer's and user's accuracies of water bodies and non-water bodies in the 'edge' stratum resulting from classification trees of Landsat data from 1999 to 2011.

	Reference classification (based on visual interpretation)			
	Water bodies	Non-water bodies	Row total	User's accuracy
Classification results				
Water bodies	183	23	206	89%
Non-water bodies	35	359	394	91%
Column total	218	382		
Producer's Accuracy	84%	94%		Overall accuracy = 90%

Table 3
The error matrix, overall, producer's and user's accuracies of water bodies and non-water bodies resulting from classification trees of Landsat data from 1999 to 2011.

	Reference classification (based on visual interpretation)			
	Water bodies	Non-water bodies	Row total	User's accuracy
Classification results				
Water bodies	396	30	426	93%
Non-water bodies	51	1323	1374	96%
Column total	447	1353		
Producer's Accuracy	89%	98%		Overall accuracy = 96%

4. Discussion and conclusions

Our study integrating time-series of Landsat data with landscape metrics identified and characterized the dynamic of surface water bodies on the SCP. We derived spatially and temporally explicit dynamics in surface water bodies and quantified the change in their numbers, extent and total area from 1999 to 2011. The opening of the USGS/EROS Landsat satellite image archive provided a unique opportunity for seasonally continuous mapping of surface water extent using time-series of moderate spatial resolution images. Seasonally continuous time-series of surface water body data are important for several analyses such as understanding how the size of water bodies changes with water abstraction, applications for landscape connectivity analysis and linking the time-series of surface water bodies with climate change data to determine how the spatiotemporal variability of the surface water bodies changes in a warming climate.

Similar to previous studies mapping wetlands and water bodies, bands 5, 4 and 3 were useful in classifying water bodies (Baker et al., 2006; Bwangoy et al., 2010; Frazier and Page, 2000; Johnston and Barson, 1993; Kingsford et al., 2004; Smith, 1997). Previous studies also found that ancillary data such as soils and DEM-derived terrain variables were important for separating wetlands from uplands (Bwangoy et al., 2010; Ozesmi and Bauer, 2002; Wright and Gallant, 2007). In this study, the variables used for mapping surface water bodies are solely based on Landsat spectral information. An SRTM-derived 90 m × 90 m digital elevation model (Rabus et al., 2003;USGS, 2006) was initially included in algorithm tests over a subset of the study area but taken out of the final model run as it only explained less than 1% of the variability while substantially increasing computation time. Major water bodies of the study area are situated in depressions between dunes but numerous small water bodies are located in small depression on a gently sloping terrain. These small depressions were not captured in the DEM tested but were captured using the spectral variables. Future development of the mapping algorithms should test a high resolution digital elevation model derived from airborne LiDAR.

Our overall accuracy of 96% for surface water bodies was similar to what previous studies have found when mapping surface water (Bwangoy et al., 2010; Wright and Gallant, 2007). It is known that a simple random sample is unlikely to provide a precise estimate of classification accuracy of a rare class unless the sample is large.

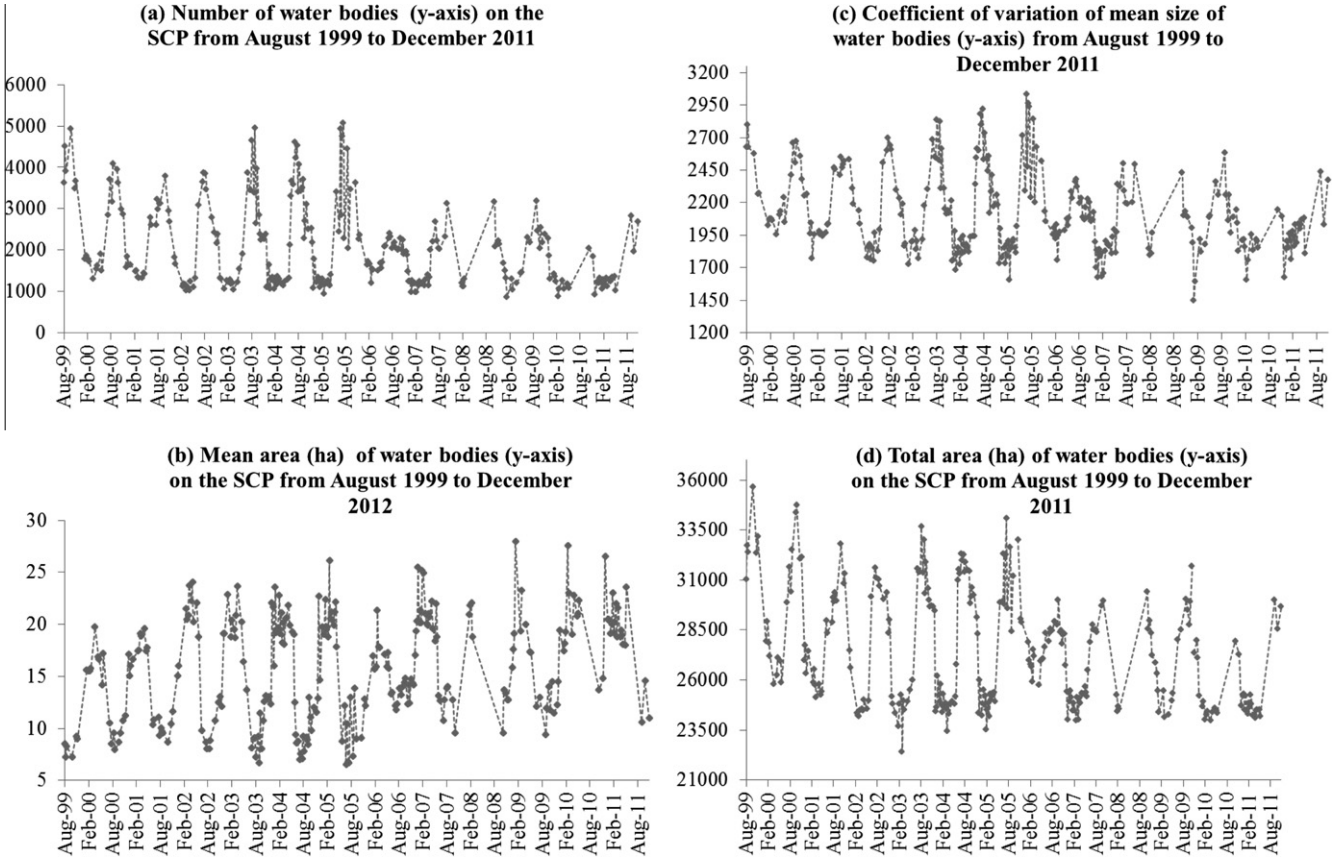

Fig. 3. (a) Number of water bodies, (b) mean area of water bodies, (c) coefficient of variation of mean area of number of water bodies and (d) total area of water bodies on the SCP landscape. It should be noted that the dotted line that unites the 278 time steps is inserted to support visualisation of dynamics only and should not be interpreted as a statistical trend.

Stratifying the SCP into the three strata to sample randomly across each area increased the number of samples representing water bodies. Increasing the number of samples along the edge of water bodies provided a robust basis for evaluating the accuracy of our surface water body time-series. Both our overall accuracies estimated from the combination of samples as well as along class boundaries were above 90%. Ideally, higher spatial resolution reference imagery would be used to evaluate the accuracy of change. Limited project resources and historic data availability did not allow us to acquire higher spatial resolution imagery suitable to represent the spatiotemporal dynamics quantified with Landsat across 36,000 km^2 and 13 years. The Landsat-based spatiotemporal accuracy assessment conducted here is sufficiently high. Further evaluation of the change in water bodies against other datasets such as ground measured water level records and precipitation data will be valuable.

The total number of water bodies showed, as anticipated, high seasonality with higher numbers of water bodies in the southern hemisphere winter, the season with the majority of rainfall, and lower in summer when rainfall is sparse, temperatures are high and the landscape is drier (Figs. 3a and 4). However, mean water body area was reduced in winter and had a higher coefficient of variation than in summer as shown in Figs. 3b, c and 4. The increased number of water bodies in winter is mainly due to seasonal filling of small and mid-sized water bodies that dry up in summer. This observation explains the seasonal pattern of the larger mean water body size and the lower coefficient of variation in summer.

A decline in number of water bodies during the winter was observed between 2005 and 2010 followed by a recent increase in 2011. 2010 was a year of exceptionally low rainfall throughout most of south-western Australia and Perth (Bureau of Meteorology, 2011). The fact that the number of water bodies declined after 2005 could be due to lower average precipitation after 2005 compared to previous years (Raupach et al., 2006, 2009).

The surface water body time-series presented in this research is timely since the latest acquisition was in 2011 and annual updates were anticipated. Therefore it can be used as the basis for understanding and quantifying the synergistic effects of climate impacts, water abstraction and urban development. SCP is undergoing rapid urban development (Hall et al., 2010) but no other recent survey of water bodies on the SCP is available. Necessary information on how to minimize the negative impacts of urban growth is pertinent for making decisions that consider how urban development might affect surface water bodies.

This information can support water and wetland management by government and urban water utilities as well as urban planning. Future work should support decisions on which wetlands should be preserved to meet conservation goals, how much of the catchment around these sites should be excluded from urban development and what groundwater abstraction rates are acceptable. The spatially explicit linkage between surface water body dynamics, ground water levels, climate, and urbanisation leading to increased ground water abstraction and reduced recharge should be investigated with the aim of informing sustainable water use policy.

Several limitations of our study should be noted. First, our method does not differentiate between surface water bodies that fill up and dry out naturally or artificially. As the hydrological cycle

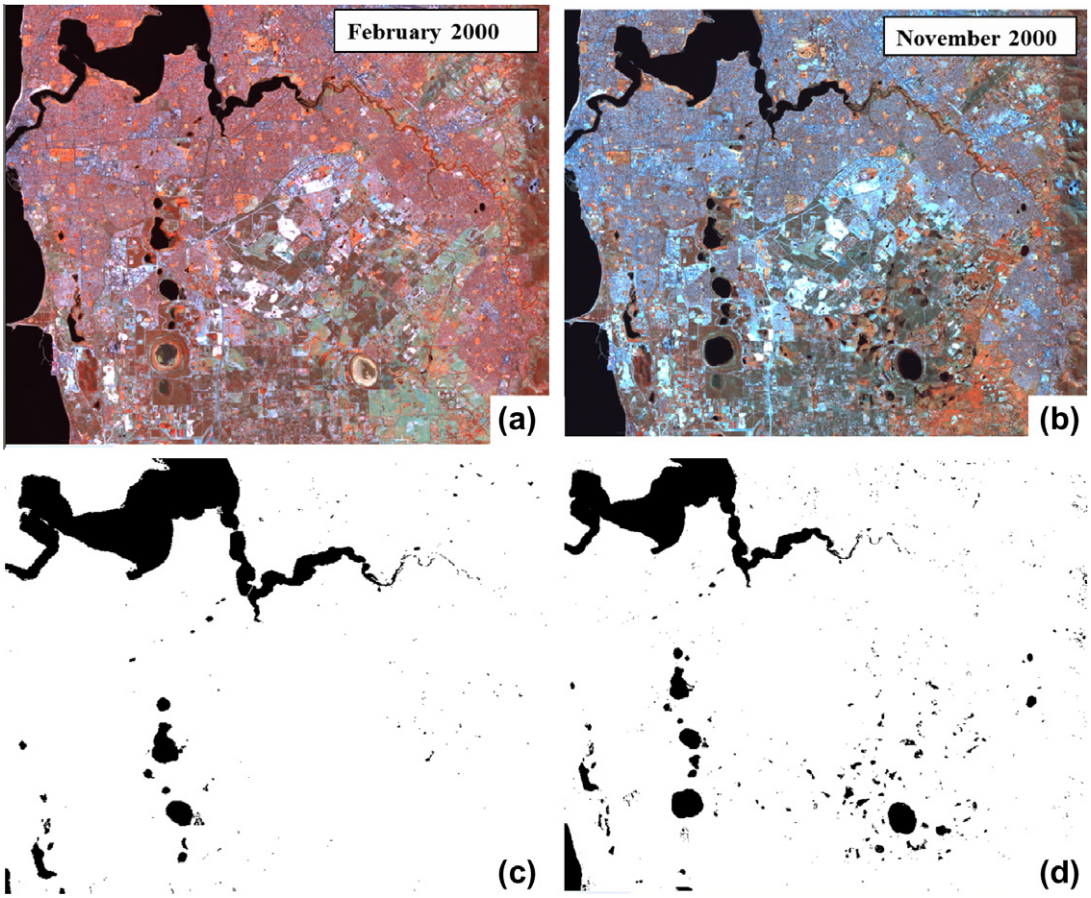

Fig. 4. Landsat images (path/row 112/082, bands 4, 5, 6 (RGB)) showing the seasonal variability as well as the results of the classification (a) summer season imagery, (b) winter season image, (c) result of the classification for the summer season and (d) result of the classification for the winter season image. Water bodies are shown in black in all images.

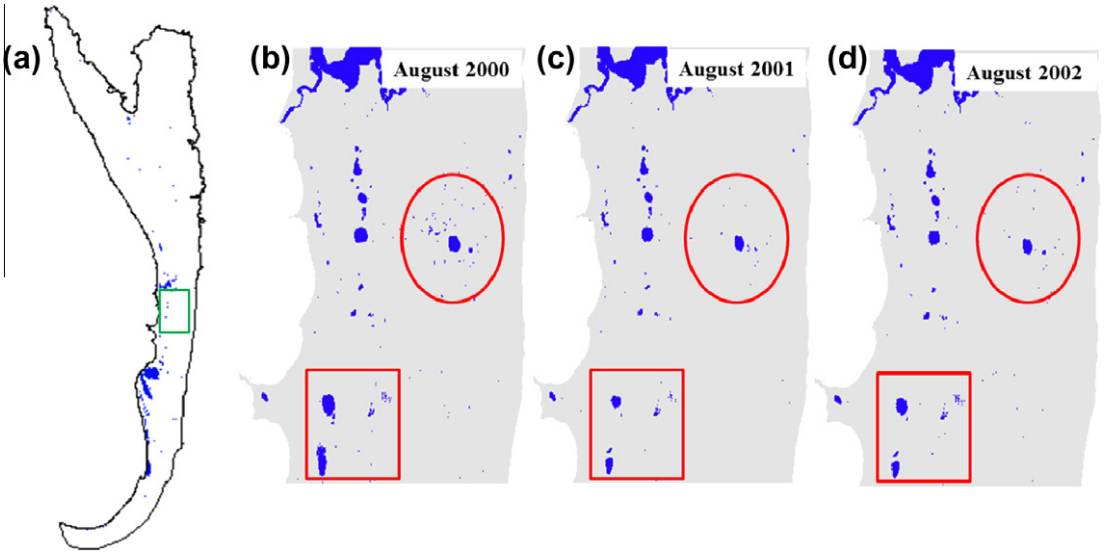

Fig. 5. Classification tree results for a subarea of the SCP south of the Swan River (inset in Fig. 5a) for three time steps (b) August 2000, (c) August 2001 and (d) August 2002 highlighting interannual differences in number of water bodies (top three circles) and in size of water bodies (bottom rectangles).

is the dominant factor influencing the physiochemical and biological processes of the surface water bodies and wetlands on the SCP (Chambers and Davis, 1989), the Environmental Protection Authority manages the water levels in a number of wetlands to prevent drying (Sommer et al., 2008). Future work should obtain spatially explicit information on water bodies where water level is artificially maintained. The surface water body data presented in this research should not be directly compared with the number of wetlands mapped by Hill et al (1996), but rather interpreted as a comparison across seasons and time. Second, we are mapping surface water bodies rather than wetlands. However, most of the wetlands on the SCP are either

shallow lakes or basin wetlands and the ability to map surface water extent is a first important step in mapping hydrological dynamics of wetlands. Future work should include mapping of fringing wetland vegetation.

Landsat satellite imagery provided appropriate spatial and temporal resolution necessary for assessing the extent and distribution of water bodies over time on the SCP. The time-series presented here should be updated as new Landsat data become available. Future work will utilize the time-series for understanding in a spatially and temporally explicit way the effect of climate, water abstraction and land use on surface water dynamic as well as assessing their connectivity for bioata in a changing climate.

Acknowledgments

We thank Stuart Kininmonth and three anonymous reviewers for helpful comments on an earlier draft.

References

Alsdorf, D.E., Rodriguez, E., Lettenmaier, D.P., 2007. Measuring surface water from space. Reviews of Geophysics 45.

Millenium Ecosystem Assessment, 2005. Ecosystems and Human Well-being. Wetlands and Water Synthesis. World Resource Institute, Washington, DC, 80p.

Baker, C., Lawrence, R., Montagne, C., Patten, D., 2006. Mapping wetlands and riparian areas using Landsat ETM+ imagery and decision-tree-based models. Wetlands 26, 465–474.

Baker, C., Lawrence, R., Montagne, C., Patten, D., 2007. Change detection of wetland ecosystems using Landsat imagery and change vector analysis. Wetlands 27, 610–619.

Braganza, K., Church, J.A., 2011. Observations of global and Australian climate. In: Cleugh, H., Smith, M.S., Battaglia, M., Graham, P. (Eds.), Climate Change: Science and Solutions for Australia. CSIRO Publishing, Collingwood, Australia, pp. 1–14.

Breiman, L., 1996. Bagging predictors. Machine Learning 24 (2), 123–140.

Breiman, L., Friedman, J.H., Stone, C.J., Olshen, R.A., 1984. Classification and Regression Trees. Chapman and Hall/CRC, Boca Raton, FL, p. 368.

Broich, M., Hansen, M., Stolle, F., Potapov, P., Margono, B.A., Adusei, B., 2011a. Remotely sensed forest cover loss shows high spatial and temporal variation across Sumatera and Kalimantan, Indonesia 2000–2008. Environmental Research Letters 6 (1).

Broich, M., Hansen, M.C., Potapov, P., Adusei, B., Lindquist, E., Stehman, S.V., 2011b. Time-series analysis of multi-resolution optical imagery for quantifying forest cover loss in Sumatra and Kalimantan, Indonesia. International Journal of Applied Earth Observation and Geoinformation 13, 277–291.

Brown de Colstoun, E.C., Story, M.H., Thompson, C., Commisso, K., Smith, T.G., Irons, J.R., 2003. National Park vegetation mapping using multitemporal Landsat 7 data and a decision tree classifier. Remote Sensing of Environment 85, 316–327.

Bureau of Meteorology, 2011. Perth in 2010: One of the Hottest and Driest Years on Record. <http://www.bom.gov.au/climate/current/annual/wa/archive/2010.perth.shtml> (last checked 26.11.12).

Bwangoy, J.R.B., Hansen, M.C., Roy, D.P., De Grandi, G., Justice, C.O., 2010. Wetland mapping in the Congo Basin using optical and radar remotely sensed data and derived topographical indices. Remote Sensing of Environment 114, 73–86.

Chambers, J.M., Davis, J.A., 1989. How wetlands work. Proceedings of the Swan Coastal Plain Groundwater Management Conference. Western Australian Water Resources, 97–103.

Chander, G., Markham, B.L., Helder, D.L., 2009. Summary of current radiometric calibration coefficients for Landsat MSS, TM, ETM+, and EO-1 ALI sensors. Remote Sensing of Environment 113, 893–903.

Cleugh, H., Smith, M.S., Battaglia, M., Graham, P. (Eds.), 2011. Climate Change: Science and Solutions for Australia. CSIRO Publishing, Collingwood, Australia, <http://j.mp/Climate_Change_pdf>.

Davis, J.A., Froend, R., 1999. Loss and degradation of wetlands in southwestern Australia: underlying causes, consequences and solutions. Wetlands Ecology and Management 7, 13–23.

Davis, J., Sim, L., Chambers, J., 2010. Multiple stressors and regime shifts in shallow aquatic ecosystems in antipodean landscapes. Freshwater Biology 55, 5–18.

Department of Sustainability, 2009. E. Water, Population and Communities. Australian Natural Resources Atlas. Biodiversity and Vegetation – Swan Coastal Plain. <http://www.anra.gov.au/topics/vegetation/extent/wa/ibra-swan-coastal-plain.html> (last accessed 26.11.12).

Exelis Visual Information Solutions, 2011. ENVI software v. 4.8.

Finlayson, C.M., Davidson, N.C., Spiers, A.G., Stevenson, N.J., 1999. Global wetland inventory – current status and future priorities. Marine and Freshwater Research 50, 717–727.

Finlayson, C.M., Davis, J.A., Gell, P.A., Kingsford, R.T., Parton, K.A., 2011. The status of wetlands and the predicted effects of global climate change: the situation in Australia. Aquatic Sciences – Research Across Boundaries, pp. 1–21.

Foody, G.M., 2002. Status of land cover classification accuracy assessment. Remote Sensing of Environment 80, 185–201.

Frazier, P.S., Page, K.J., 2000. Water body detection and delineation with Landsat TM data. Photogrammetric Engineering and Remote Sensing 66 (12), 1461–1467.

Friedl, M.A., Brodley, C.E., 1997. Decision tree classification of land cover from remotely sensed data. Remote Sensing of Environment 61, 399–409.

Froend, R., Sommer, B., 2010. Phreatophytic vegetation response to climatic and abstraction-induced groundwater drawdown: examples of long-term spatial and temporal variability in community response. Ecological Engineering 36, 1191–1200.

Frohn, R., Reif, M., Lane, C., Autrey, B., 2009. Satellite remote sensing of isolated wetlands using object-oriented classification of Landsat-7 data. Wetlands 29, 931–941.

Hall, J., Kretschmer, P., Quinton, B., Marrilier, B., 2010. Murray hydrological studies: surface water, groundwater and environmental water – land development, drainage and climate scenario report. In: Water Science Technical Series, vol.: WST26. Department of Water, Government of Western Australia, 100p.

Hansen, M.C., Loveland, T.R., 2012. A review of large area monitoring of land cover change using Landsat data. Remote Sensing of Environment 122, 66–74.

Hansen, M.C., Roy, D.P., Lindquist, E., Adusei, B., Justice, C.O., Altstatt, A., 2008. A method for integrating MODIS and Landsat data for systematic monitoring of forest cover and change in the Congo Basin. Remote Sensing of Environment 112, 2495–2513.

Hill, A.L., Semeniuk, C.A., Semeniuk, V., Del Marco, A., 1996. Wetlands of the Swan Coastal Plain. Wetland mapping, classification, and evaluation, main report Water and Rivers Commisision and the Department of Environmental Protection, Perth, Western Australia, vol. 2AL, 146p.

Horwitz, P., Bradshaw, D., Hopper, S., Davies, P., Froend, R., Bradshaw, F., 2008. Hydrological change escalates risk of ecosystem stress in Australia's threatened biodiversity hotspot. Royal Society of Western Australia 91 (1), 1–11.

Johnston, R.M., Barson, M.M., 1993. Remote sensing of Australian wetlands: an evaluation of Landsat TM data for inventory and classification. Australian Journal of Marine and Freshwater Research 44, 235–252.

Kingsford, R.T., Brandis, K., Thomas, R.F., Crighton, P., Knowles, E., Gale, E., 2004. Classifying landform at broad spatial scales: the distribution and conservation of wetlands in New South Wales, Australia. Marine and Freshwater Research 55, 17–31.

Maxwell, S.K., Schmidt, G.L., Storey, J.C., 2007. A multi-scale segmentation approach to filling gaps in Landsat ETM+ SLC-off images. International Journal of Remote Sensing 28, 5339–5356.

McGarigal, K., Cushman, S.A., Neel, M.C., Ene, E., 2002. FRAGSTATS: Spatial Pattern Analysis Program for Categorical Maps. Computer software program produced by the authors at the University of Massachusetts, Amherst. <http://www.umass.edu/landeco/research/fragstats/fragstats.html>.

Mitsch, W.J., Gosselink, J.G., 1993. Wetlands. Van Nostrand Reinhold, New York, NY, 539p..

Ozesmi, S.L., Bauer, M.E., 2002. Satellite remote sensing of wetlands. Wetlands Ecology and Management 10, 381–402.

Pressey, R.L., Adam, P., 1995. A review of wetland inventory and classification in Australia. Plant Ecology 118, 81–101.

R Development Core Team, 2008. R.

Rabus, B., Eineder, M., Roth, A., Bamler, R., 2003. The shuttle radar topography mission-a new class of digital elevation models acquired by spaceborne radar. Journal of Photogrammetry and Remote Sensing 57, 241–262.

Raupach, M.R., Briggs, P.R., Haverd, V., King, E.A., Paget, M., Trudinger, C.M., 2006. Australian Water Availability Project. CSIRO Marine and Atmospheric Research. Canberra, Australia, 44p.

Raupach, M.R., Briggs, P., Haverd, V., King, E.A., Paget, M., Trudinger, C.M., 2009. Australian Water Availability Project (AWAP): CSIRO Marine and Atmospheric Research Component: Final Report for Phase 3. CAWCR Technical Report 13, 72p.

Roy, D.P., Ju, J.C., Kline, K., Scaramuzza, P.L., Kovalskyy, V., Hansen, M., Loveland, T.R., Vermote, E., Zhang, C.S., 2010. Web-enabled Landsat Data (WELD): Landsat ETM plus composited mosaics of the conterminous United States. Remote Sensing of Environment 114, 35–49.

Semeniuk, C.A., Semeniuk, V., 1995. A geomorphic approcah to global classification for inland wetlands. Vegetatio 118, 103–124.

Smith, L.C., 1997. Satellite remote sensing of river inundation area, stage, and discharge: a review. Hydrol Process 11, 1427–1439.

Smith, J.H., Stehman, S.V., Wickham, J.D., Yang, L., 2003. Effects of landscape characteristics on land-cover class accuracy. Remote Sensing of Environment 84, 342–349.

Sommer, B., Horwitz, P., 2009. Macroinvertebrate cycles of decline and recovery in Swan Coastal Plain (Western Australia) wetlands affected by drought-induced acidification. Hydrobiologia 624, 191–203.

Sommer, B., Horwitz, P., Hewitt, P., 2008. Assessment of wetland invertebrate and fish biodiversity for the Gnangara Sustainability Strategy (GSS). Centre for Ecosystem Management. Edith Cowan University, Joondalup, WA, 123p..

Stehman, S.V., Czaplewski, R.L., 1998. Design and analysis for thematic map accuracy assessment: fundamental principles. Remote Sensing of Environment 64, 331–344.

Stehman, S.V., Wickham, J.D., Smith, J.H., Yang, L., 2003. Thematic accuracy of the 1992 National Land-Cover Data for the eastern United States: statistical methodology and regional results. Remote Sensing of Environment 86, 500–516.

Townley, L.R., lhrner, J.V., Barr, A.D., Trefry, M.G., Wright, K.D., Gailitis, V., Harris, C.J., Johnson, C.D., 1993. Wetlands of the Swan Coastal plain: vol. 3: Interactions between lakes, wetlands and unconfined aquifers. Water Authority of Western Australia, 115p.

UNESCO 1971. Article 1, Part 1, Convention on wetlands of international significance. Published in Australia in 1976 for the Department of Foreign Affairs. Australian Government Publishing Service, Treaty Series 1975, No. 48.

USGS, 2003. Landsat: a global land-observing program. U.S. Geological Survey, Reston, VA, USA. USGS Factsheet 023-63, 4p.

USGS, 2006. Shuttle Radar Topography Mission, 3 Arc Second, Filled Finished-A, 2.0, Global Land Cover Facility, University of Maryland, College Park, Maryland.

Weller, R., 2009. Boomtown 2050: Scenarios for a Rapidly Growing City UWA Publishing.

Williams, D.L., Goward, S., Arvidson, T., 2006. Landsat: Yesterday, today, and tomorrow. Photogrammetric Engineering and Remote Sensing 72 (10), 1171–1178.

Wright, C., Gallant, A., 2007. Improved wetland remote sensing in Yellowstone National Park using classification trees to combine TM imagery and ancillary environmental data. Remote Sensing of Environment 107, 582–605.

Zedler, J.B., Kercher, S., 2005. Wetland resources: status, trends, ecosystem services, and restorability. Annual Review of Environment and Resources 30, 39–74.